RESEARCH

Optical parametric oscillator and amplifier providing tunable, narrowband nanosecond laser pulses in the mid-infrared with mJ pulse energy

Jan Frederic Kinder[1] · Benedikt Moneke[1] · Oskar Ernst[1] · Thomas Halfmann[1]

Abstract

We report on an all-solid-state light source for nanosecond (ns) laser pulses, with broad tunability in the mid-infrared, spectral bandwidth close to the Fourier transform limit, and pulse energy in the mJ regime. To this end, we extend a tunable, continuous wave (cw) singly resonant optical parametric oscillator by an optical parametric pre-amplifier with a periodically poled lithium niobate crystal and a power amplifier stage with two bulk lithium niobate crystals. We demonstrate pulse energies beyond 1 mJ in a tuning range between 3.3 and 3.8 µm center wavelength, with options for even larger output pulse energy and tuning range. The total conversion efficiency in the power amplifier reaches 20%. From measurements of absorption spectroscopy, we determine a very narrow linewidth of 108 MHz (full width at half maximum, FWHM), which is only a factor of 1.4 above the Fourier limit. We demonstrate the applicability and versatility of the laser system for nonlinear spectroscopy by resonantly enhanced third harmonic generation and sum frequency mixing in a gas sample of HCl molecules.

1 Introduction

Sensitive molecule detection by nonlinear optical spectroscopy via vibrational states requires light sources for mid-infrared laser pulses with continuous tunability, narrow spectral bandwidth (close to the Fourier transform limit) and high pulse energy.

With regard to the pulse duration, nanosecond (ns) pulses typically offer the best combination of still sufficiently narrow bandwidth to selectively address rovibrational transitions and large pulse energy (or intensity) to drive nonlinear interactions. There are a few approaches, usually involving nonlinear optical frequency conversion processes, to generate such tunable, intense, mid-infrared (ns) laser pulses with pulse energies in the mJ regime. Examples are difference frequency mixing of visible radiation from tunable dye lasers [1, 2] or generation of mid-infrared radiation directly from optical parametric oscillators (OPOs) [3]. While dye laser systems are typically rather large, as well as difficult to handle and embed in realistic applications of nonlinear

spectrometry, OPOs as compact and robust all-solid-state devices are an attractive solution for such purposes. In the OPO process, a pump field creates a signal and idler wave by difference frequency conversion. For a visible or near-infrared pump wave, the lower frequency idler wave is in the mid-infrared spectral range. Phase matching allows for broad tunability of such devices. The OPO process takes place in a cavity to enhance the conversion efficiency and to allow for mode selection.

Since periodically poled lithium niobate (PPLN) became available as a medium with large nonlinear susceptibility and large interaction length due to operation under conditions of quasi-phase matching, the implementation of continuous wave (cw) singly resonant OPOs to deliver narrowband, mid-infrared radiation with high beam quality became possible [4–7]. The (cw) OPO devices are broadly tunable in ranges of many 100 nm (or beyond), permit single longitudinal mode operation, and output power reaching several Watt. In a recent, related approach, a broadly tunable diode laser was applied to seed an (cw) OPO system [8].

Thus, (cw) OPO-based mid-infrared sources are meanwhile readily available. However, there are so far only very few (ns) OPO-based laser systems, which combine broad continuous tunability with Fourier-limited spectral bandwidth and large pulse energy. In particular, providing for single longitudinal mode operation in a broadly tunable, pulsed

---

✉ Jan Frederic Kinder
  jan-frederic.kinder@physik.tu-darmstadt.de

1   Institut für Angewandte Physik, Technische Universität Darmstadt, Hochschulstr. 6, 64289 Darmstadt, Germany

OPO is a severe challenge [9]. Bosenberg and Guyer [10] reported on a (ns) OPO with an intracavity grating to operate on a single longitudinal mode. Extended by additional difference frequency mixing stages, the rather complex system allowed the generation of continuously tunable mid-infrared (ns) pulses with wavelengths of 1.3–4 μm at pulse energies in the mJ range, but still at a large bandwidth of 500 MHz.

While injection seeding of pulsed OPOs may serve to efficiently reduce the bandwidth, it does usually not provide broad tunability and requires precise mode matching of the seed laser with the OPO cavity. In such an approach, Baxter and Orr [11] set up a (ns) OPO, involving injection seeding by a tunable diode laser. The signal output of the OPO seeded an optical parametric amplifier, to generate (ns) pulses with a spectral bandwidth approaching the Fourier limit. The system reached a combined pulse energy of 2 mJ for the signal and idler output. At an idler wavelength of 3.4 μm this corresponds to an idler pulse energy of 0.6 mJ, i.e., at least approaching the mJ regime. However, due to the limited tunability, the authors demonstrated operation at a fixed idler wavelength only.

Optical parametric generators (OPG) were considered as an alternative [12]. In such devices, amplification of vacuum fluctuations produces measurable output even after a single pass through the nonlinear crystal, without the need for a cavity. However, due to the large acceptance bandwidth of the OPG process, the output radiation has huge spectral bandwidth—which exceeds the Fourier transform limit for (ns) pulses by orders of magnitude. Powers et al. demonstrated spectral filtering of the OPG output with an etalon to provide seed radiation for a second stage OPA process [13]. While the system only requires a single pump laser, the etalon prohibits broad tunability. Furthermore, the free spectral range of the etalon limited the bandwidth of the idler pulses to ≈ 1.8 GHz, i.e., much larger than the Fourier-limited bandwidth. Bäder et al. used a temperature-tuned laser diode as seed source to reduce the spectral bandwidth of the OPG process down to 140 MHz [14]. However, while the setup reached at least a pulse energy of 0.76 mJ, also this approach did not provide broad tunability (similar to seeding an OPO, see above) and the beam quality (measured in terms of M^2) was far from the diffraction limit.

In the following, we present a setup for a (ns) OPO laser system, which involves a (cw) OPO as a broadly tunable seed source for two subsequent optical parametric amplifier (OPA) stages, pumped by a (ns) laser. In an OPA, the seed radiation is amplified, along with generation of signal or idler radiation at the corresponding wavelength. This approach allows the generation of widely tunable (ns) pulses in the mid-infrared, with spectral bandwidth close to the Fourier transform limit, and large output pulse energy in the mJ regime, along with very good beam quality. As an additional attractive feature for spectroscopic applications, (cw)

and (ns) mid-infrared radiation are simultaneously available. We thoroughly characterize the laser system, also involving determination of its spectral bandwidth by absorption spectroscopy, and verification of the narrow bandwidth by nonlinear spectroscopy in molecular species.

2 Experimental setup

Figure 1 shows the setup of the OPO/OPA laser system. We apply a commercial (cw) singly resonant optical parametric oscillator (OPO, Argos Model 2400-C, Aculight/Lockheed Martin), pumped by a fiber amplifier (YAR-15K-1064-LP-SF, IPG Photonics), seeded with an external fiber laser oscillator (Koheras Basik Y10, NKT Photonics) at a wavelength of 1064 nm. The (cw) OPO delivers output powers in the range of 1 W across an idler tuning range between 3.2 and 3.9 μm (for the specific OPO module, other wavelength intervals in the mid-infrared are accessible with other OPO modules of the Argos system). An intracavity etalon selects a single longitudinal mode. Mode hop free fine tuning of the idler output is established by tuning the pump fiber laser wavelength. The spectral bandwidth is specified ≤ 1 MHz (full width at half maximum, FWHM) [7]. We modified the commercial OPO to enable computer-controlled wavelength tunability [15]. For spectroscopic investigations and wavelength calibration, we detect a small fraction of the (cw) OPO idler output with a home-made grating spectrometer. By spectroscopic investigations in HCl we confirmed, that the amplified (ns) pulses have the same central wavelength as the (cw) OPO idler radiation (see discussion in Sect. 3.2). We note, that in the meantime we build the (cw) OPO modules with a home-made design ourselves, to improve robustness, applicability, and wavelength coverage. However, we conducted all measurements presented below still with the commercial (cw) OPO.

The idler wave from the (cw) OPO propagates into the first OPA stage (pre-amplifier), implemented by a PPLN crystal (dimensions: $50 \times 12 \times 1$ mm^3, anti-reflection coated for all involved fields, HC Photonics). The crystal contains 7 different sections with quasi-phase matching periods ranging from 27.17 to 30.45 μm. This design provides tunability between 3.2 and 4.6 μm idler wavelength (i.e., even beyond the wavelength range of the (cw) OPO module applied here) via a temperature control unit (HC Photonics), which covers the range from room temperature up to 200 °C. To omit photorefractive damage, the substrate is doped with 5 % Magnesium oxide (MgO) [16]. An injection-seeded Nd:YAG laser (Quanta-Ray PRO 230, Spectra Physics, equipped with a ROCK fiber laser seeder, NP Photonics), providing pulses with a duration of 8 ns (FWHM) at 1064 nm, Fourier transform limited bandwidth of 55 MHz, pulse repetition rate of 20 Hz, and maximal pulse energy of 1.3 J serves as
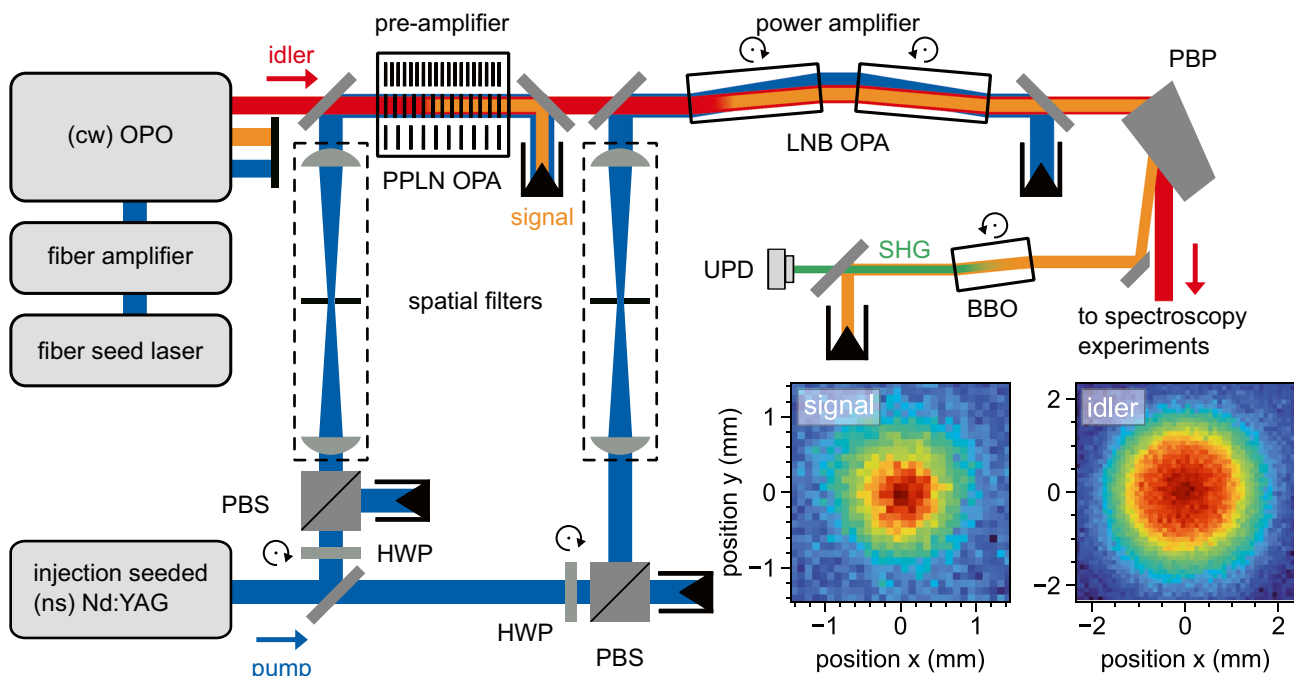
Fig. 1 Schematic overview of the laser setup with polarizing beam-splitter (PBS), half-wave plate (HWP), Pellin-Broca prism (PBP), and an ultra-fast photodetector (UPD). The inset shows the beam profiles of the signal output at $\lambda_{signal} = 1521$ nm and the corresponding mid-infrared idler output at $\lambda_{idler} = 3543$ nm, measured behind the LNB OPA stage (red depicts large intensity, blue low intensity)

pump source for both OPA stages. We use a spatial filter to improve the Gaussian profile of the pump beam. We collimate the pump radiation to a $1/e^2$-diameter of ≈ 0.83 mm and mildly focus the (cw) mid-infrared seed radiation with a diameter of ≈ 0.65 mm into the PPLN crystal. The typical pump pulse energy was 0.5 mJ, limited by the damage threshold of the PPLN crystal. Dichroic mirrors on CaF_2 substrate (Laseroptik) serve to combine and separate pump and idler radiation. Due to the large effective nonlinear susceptibility, a PPLN-based OPA might suffer from gain guiding and self-focussing in the crystal [17]. We noticed somewhat large divergence for the mid-infrared OPA output and slightly reduced beam quality.

After the PPLN OPA, we further amplify the mid-infrared pulse energy in a second OPA stage (power amplifier). To prohibit back conversion, we remove the near-infrared signal output of the PPLN OPA with a spectral longpass filter (#68-653, Edmund Optics). The second OPA stage consists of two 3 cm long bulk lithium niobate (LNB) crystals, doped with 5 % MgO (supplied by Castech), cut at type I phase matching angles $\theta = 45°$ and $\phi = 30°$. We note, that PPLN would not be applicable at the large pulse intensities in the power amplifier due to the low damage threshold of the PPLN substrate, combined with the limited crystal thickness. Thus, we use bulk LNB. In an earlier version of our setup, we noticed oscillations of the idler pulse energy, when we varied the wavelength. These were probably due to etalon effects for idler and signal

wave in the power amplifier stage. Hence, the crystal apertures are anti-reflection coated and have 0.5 ° wedges to prevent back reflections and oscillations. We operated the power amplifier with a typical pump pulse energy of 23 mJ, limited by the damage threshold of the dichroic combiner mirrors. The pump field experiences a walk-off of 2.1 °. To cope with this, we arrange the two crystals of the power amplifier stage in walk-off compensation geometry [18]. The pump and seed beam $1/e^2$-diameters in the crystal are 1.6 mm and 3.9 mm, respectively. With the larger seed beam profile, we ensure spatial overlap throughout the crystals. We note that this configuration might lead to perturbations in the idler beam profile due to the pump beam walk-off. We chose this setup due to technical limitations of the spatial filter for the pump radiation, in combination with the low damage threshold of the dichroic combiner mirror. After the OPA stages, a Pellin-Broca prism separates the mid-infrared idler pulses from the near-infrared signal pulses, residual pump radiation and other parasitic nonlinear processes, which occur in the LNB crystals.

3 Experimental results

3.1 Characterization of the OPA stages

We measure the beam profiles for the signal and idler output of the LNB OPA stage with a home-made moving-aperture

beam profiler, involving a pinhole of diameter 100 μm (P100H, Thorlabs) and a photovoltaic InAsSb detector (P13243-011MA, Hamamatsu Photonics) to determine the transmitted pulse energy. The inset in Fig. 1 shows the profiles of the (ns) signal and idler beams after the LNB OPA stage (power amplifier). Both beams have nice Gaussian shapes, with $1/e^2$-radii of ≈ 1.1 mm (signal) and ≈ 2.2 mm (idler). The difference is due to the wavelength dependence of the beam divergence.

As we could not measure the pulse duration of mid-infrared pulses directly, we measured the second harmonic of the signal pulses instead and estimated the idler pulse duration from the data. In the measurement, the idler had a wavelength of 3547 nm. With a pump wavelength of 1064 nm, we calculate the signal wavelength as 1520 nm, and its second harmonic at 760 nm. We generate the second harmonic in a 12 mm long Beta Barium Borate (BBO) crystal (Castech) and detect its temporal profile on an ultra-fast photodetector (UPD-200-UD, Alphalas). The pulse trace has a Gaussian temporal shape with a duration (FWHM) of 4.2 ns. The rise time and resolution of the detection and digitization setup is ≈ 1 ns. Hence, the actual second harmonic pulse duration is 4.1 ns. This corresponds to a signal pulse duration of 5.8 ns. Assuming, that the gain in the power amplifier stage is large (i.e., well beyond one), we may expect equal pulse durations for signal and idler. We also verified this assumption with a numerical simulation using SNLO [19].

We turn our attention now to the tuning characteristics of the OPA stages. As the pre-amplifier stage relies on quasi-phase matching, we require variation of the temperature for different poling periods. Figure 2a shows the measured quasi-phase matching temperature in the PPLN OPA vs. idler wavelength. Three sections on the PPLN crystal with poling periods of 30.45, 29.8, and 29.25 μm cover the wavelength tuning range depicted in the figure. A calculation based on the temperature dependent refractive index of 5 % MgO-doped LNB [20] and coefficients for thermal expansion [21, 22] describes the experimental results very well.

Figure 2b shows the measured phase matching angle in the LNB OPA vs. idler wavelength. As the power amplifier relies on critical phase matching, we require angle tuning of the LNB crystals. For this task, we use computer controlled stepper motors as actuators. The angle values in Fig. 2 take refraction at the air-crystal interface into account [20]. We use the phase matching angle of $\theta = 45°$, corresponding to an idler wavelength of 3500 nm, as reference. The experimental data agrees very well with a calculation based upon the refractive index of 5 % MgO-doped LNB [20].

Already obvious from the latter results, the OPA stages permit generation of mid-infrared (ns) pulses throughout the whole tuning range of the (cw) OPO. We will consider now the achieved pulse energy. Figure 3a shows the idler power
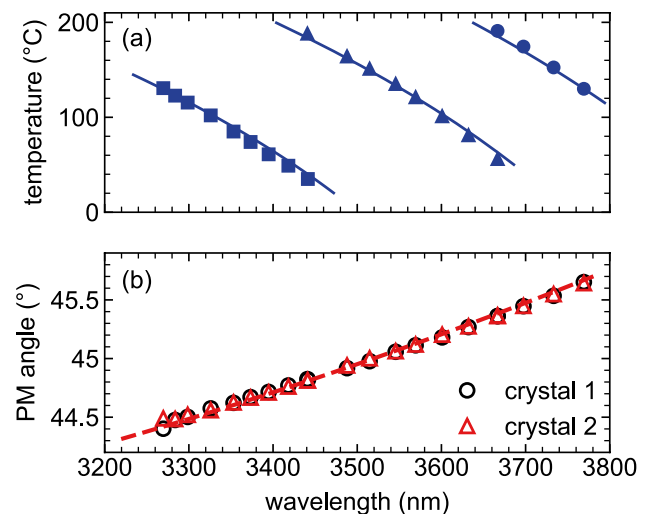

Fig. 2 **a** Quasi-phase matching temperature for the PPLN crystal versus (cw) seed wavelength. Blue squares, triangles, and circles indicate phasematching periods 30.45 μm, 29.8 μm, and 29.25 μm, respectively. Lines indicate the expectation. **b** Internal phase matching (PM) angle for both LNB crystals of the LNB OPA stage versus (cw) seed wavelength. The dashed line indicates the expectation

of the (cw) seed OPO, which serves as input to the OPAs. The seed power is larger than 0.75 W over the whole tuning range. It drops at larger wavelengths, which fits with the specifications of the commercial OPO module and is probably due to the coatings of the cavity mirrors. We will discuss the effect of the (cw) seed power upon the OPA performance in more detail below. Let us consider now the obtained (ns) idler pulse energy after amplification (see Fig. 3b), measured with a pyroelectric energy meter (PE10-C, Ophir). The PPLN OPA stage (pre-amplifier) provides idler pulse energies in the range of 30 μJ over the whole wavelength range. The LNB OPA stage (power amplifier) delivers idler pulse energies of more than 1.2 mJ with a peak pulse energy of 1.7 mJ at 3570 nm. We noticed lower idler pulse energies of the pre-amplifier stage when we operate at low quasi-phase matching temperatures ≤ 50 °C (see data points at wavelength 3440 and 3660 nm). This is probably due to temperature fluctuations or gradients in the PPLN crystal, which decrease the efficiency of the amplification process. For realistic applications, we would operate at poling periods matched to higher temperatures (compare Fig. 2a). The output pulse energy of both OPA stages slightly drops at the edges of the tuning range, which is probably due to the wavelength dependent transmission of various optical elements in the beam path. Nevertheless, we maintain a pulse energy beyond 1 mJ for all idler wavelengths.

We consider now the amplification in the two OPA stages separately. In particular, we investigated the dependencies of the idler pulse energy vs. seed and pump pulse energy. We perform these measurements at a fixed
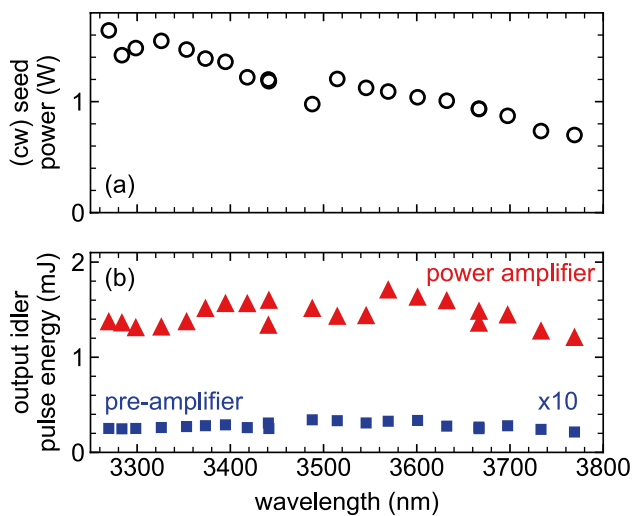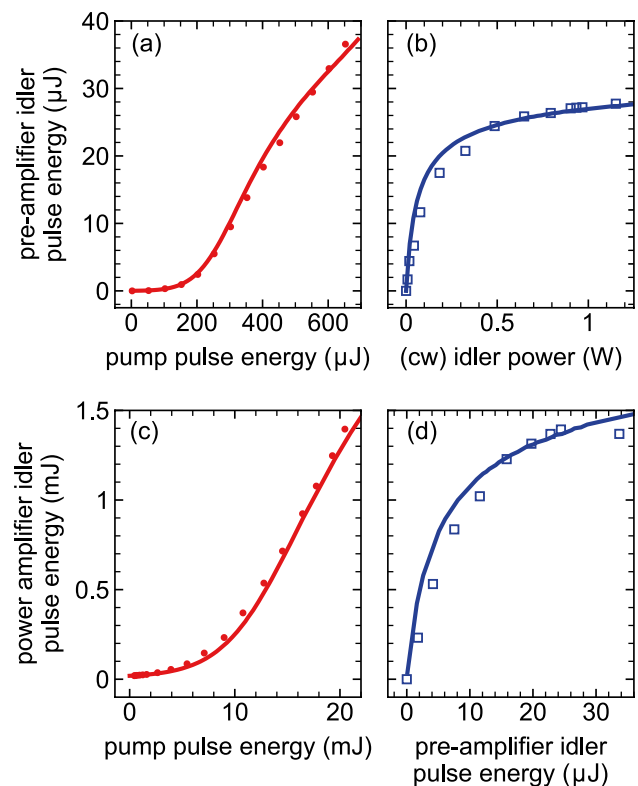
Fig. 3 a (cw) seed power versus (cw) OPO wavelength. **b** Output mid-infrared idler pulse energy versus (cw) OPO wavelength. Red triangles indicate the output of the power amplifier OPA, blue squares give the corresponding output of the pre-amplifier PPLN OPA (note the scale factor of 10). The pump pulse energies for the PPLN OPA were 0.51 mJ and for the second-stage OPA 22.9 mJ. We compensate the pulse energies for transmission losses in optical elements before the energy meter

Fig. 4 a Output mid-infrared idler pulse energy of the PPLN OPA stage versus pump pulse energy with a seed power of 0.96 W (red points). **b** Output idler pulse energy versus seed power with a pump pulse energy of 499 μJ (blue squares). **c** Output mid-infrared idler pulse energy of the LNB OPA stage versus pump pulse energy with a seed pulse of 28.6 μJ (red points, the PPLN OPA pump pulse energy was 560 μJ). **d** Output idler pulse energy versus seed pulse energy with a pump pulse energy of 22.8 mJ (blue squares). The (cw) seed wavelength was 3545 nm. We corrected the pulse energies for absorption losses. Lines indicate a numerical simulation, divided by a factor of 1.65 (pre-amplifier) and 1.90 (power amplifier)

idler seed wavelength of $\lambda_{\mathrm{idler}} = 3545$ nm. We vary the pump pulse energy with a variable attenuator, which consists of a half-wave plate and a polarising beamsplitter cube, and measure the pump pulse energies for the OPA stages with calibrated photodiodes. An energy meter detects the mid-infrared output idler pulse energy (PE10-C, Ophir). The red data points in Fig. 4a show the idler pulse energy vs. pump pulse energy, while we keep the (cw) seed power fixed at 0.96 W. The latter corresponds to a seed pulse energy of ≈ 8.1 nJ during the pump pulse. At a pump pulse energy of 650 μJ the PPLN OPA (pre-amplifier) delivers an idler pulse energy of ≈ 37 μJ. This corresponds to a single pass gain of $\approx 4.6 \times 10^3$. We do not observe significant saturation. Hence, the process is still far below threshold. We compare our results with a numerical simulation based on SNLO [19]. It fits very well with the variation of the measured idler vs. pump pulse energy. We note, that there is a constant scale factor < 2 between simulation and experimental data, which is probably due to non-perfect Gaussian beam profiles or beam overlap, and parasitic nonlinear processes.

Note, that the PPLN OPA also produces a signal output at $\lambda_{\mathrm{signal}} = 1520$ nm. As the photon energy scales with $1/\lambda$, for an idler pulse energy of ≈ 37 μJ we expect a corresponding signal pulse energy of ≈ 85 μJ. Hence, the total conversion efficiency of the pre-amplifier stage is $\approx 19\%$. This value is lower than our expectation of 30 %, as estimated with SNLO [19].

We also varied the power of the (cw) seed, while keeping the pump pulse energy fixed at 499 μJ (see blue data points in Fig. 4b). For small seed power, the idler pulse energy increases roughly linear—as expected for difference frequency mixing in the non-depleted pump approximation. For larger seed power, the process saturates. This is an important feature, which we already saw in the tuning behaviour (compare edges of the tuning range in Fig. 3): The large amplification in the PPLN OPA already smoothens variations in the seed power, e.g., across the wavelength tuning range. The data also indicates, that we may expect comparable performance of the pre-amplifier stage also for seed laser sources with lower output powers in the mW range. Again, the numerical simulation qualitatively describes the experimental data.

Let us turn now to the power amplifier stage. The red data points in Fig. 4c show the idler pulse energy after the LNB OPA stage vs. pump pulse energy, while we keep the

seed pulse energy (i.e., the output of the pre-amplifier stage) fixed at 28.6 μJ. We see no sign of saturation here. Hence, also the second OPA stage operates far below threshold. On the other hand, the dependence of the idler pulse energy vs. seed pulse energy from the pre-amplifier (see blue data points in Fig. 4d), while keeping the pump pulse energy fixed at 22.8 mJ shows the steep rise for low seed energies and saturation for large values, as also observed in the pre-amplifier. For seed pulse energies larger than ≈ 20 μJ the idler pulse energy is almost constant—which again helps to keep the idler pulse energy constant also when the seed power varies. Larger pump energy for the power amplifier or additional OPA stages would further increase the idler pulse energy. The numerical simulation based on SNLO confirms these findings.

In our measurement, we reach a maximal idler pulse energy of 1.37 mJ for a pump pulse energy of 22.8 mJ and a seed pulse energy of 33.7 μJ. This corresponds to a single pass gain of ≈ 41. From the idler pulse energy, we calculate a corresponding signal pulse energy of 3.2 mJ. Thus, with regard to the combined idler and signal pulse energy, our system operates in the regime of several mJ—with the option to proceed further at larger pump pulse energy. The total conversion efficiency in the LNB OPA stage is $\approx 20\%$, i.e., similar to the PPLN OPA stage. We'd expect similar performance of the laser system, if we seed the power amplifier stage with signal rather than idler pulses from the pre-amplifier stage. This might be relevant for operation in other wavelength regimes or with other (cw) OPO seed sources.

3.2 Determination of the linewidth by molecular spectroscopy

We proceed now to demonstrate the narrow spectral bandwidth of the mid-infrared laser pulses from our OPO/OPA laser system. To do so, we apply the laser pulses for simple absorption spectroscopy and two variants of nonlinear spectroscopy in hydrogen chloride (HCl) molecules. The latter experiments on nonlinear spectroscopy also prove the applicability of the laser system for such purposes of applied nonlinear optics. HCl is relevant in combustion processes, e.g., waste incineration of polyvinyl chloride (PVC) compounds [23] or biomass [24]. In a first series of measurements, we perform absorption spectroscopy at a rovibrational transition between the vibrational ground state $v = 0$ and the first excited state $v = 1$ of HCl molecules in a gas cell. The resonance is at a wavelength of 3546.65 nm in the isotope $H^{37}Cl$ [25]. We apply either amplified (ns) idler pulses or (cw) OPO seed radiation. The radiation passes a simple gas cell (length 18 cm) with wedged CaF_2 windows (WW51050, Thorlabs). The cell contains HCl molecules at a low pressure of 0.09 mbar. The power or pulse energy is measured before and after the cell with an InAsSb detector.

At low HCl pressure, the natural linewidth and collisional self-broadening are negligible compared to Doppler broadening. Thus, we get a Gaussian-shaped spectral profile of the absorption line.

The blue data points in Fig. 5b show the absorption spectrum obtained with narrowband (cw) radiation. The spectral bandwidth of the Gaussian function fitted to the (cw) absorption data is 190 MHz (here and in the following we will define all spectral bandwidths as FWHM). This agrees well with the expected Doppler width of 170 MHz. Note, that a Voigt profile might be inaccurate to describe the spectral line shape at low absolute pressures, as collisions effect the spectral line shape even when collisional broadening is rather negligible [26, 27].

The laser linewidth < 1 MHz of the (cw) OPO is far below the Doppler width. Hence, it is negligible for the determination of the (ns) linewidth in the following. We verified, that the OPO operated at a single longitudinal mode. This enables us to use the (cw) measurement as reference to determine the spectral bandwidth of the amplified (ns) laser pulses, which will add to the linewidth of the molecular resonance. We apply now the (ns) pulses from the full OPO/OPA system for absorption spectroscopy (see red triangles in Fig. 5b). Because of the larger spectral bandwidth, the peak absorption is lower than for narrowband (cw) radiation. From a Gaussian fit to the data, we determine a spectral bandwidth of 219 MHz. Deconvolution using the reference spectrum yields a spectral bandwidth of ≈ 108 MHz for the (ns) pulses. From the pulse duration of ≈ 5.8 ns for the amplified idler pulses, we calculate a Fourier limited bandwidth of 76 MHz, i.e., close to the value measured in absorption spectroscopy.

We also measured an absorption spectrum for the (ns) idler output of the PPLN pre-amplifier stage (data not shown in the figure). We derive a FWHM of 200 MHz from the Gaussian fit, i.e., a spectral bandwidth of ≈ 62 MHz for the (ns) pulses from the pre-amplifier. Again, this value is very close to 55 MHz for a Gaussian laser pulse with a pulse duration around 8 ns, which we roughly expect for mixing the 8 ns long pump pulse with (cw) seed radiation in the pre-amplifier stage.

In a second series of spectroscopic measurements, we demonstrate the applicability of the OPO/OPA laser system for nonlinear optical spectroscopy. In other work, we already investigated molecule detection by third harmonic generation (THG), resonantly enhanced by rovibrational resonances in HCl, driven by our (ns) mid-infrared light source [28]. We performed a similar experiment now, with an emphasis to determine the laser linewidth from THG spectra. Figure 5a gives the relevant rovibrational energy levels of the electronic ground state in $H^{35}Cl$. When intense mid-infrared laser pulses at a wavelength of 3.533 μm interact with the molecules, the fundamental radiation drives
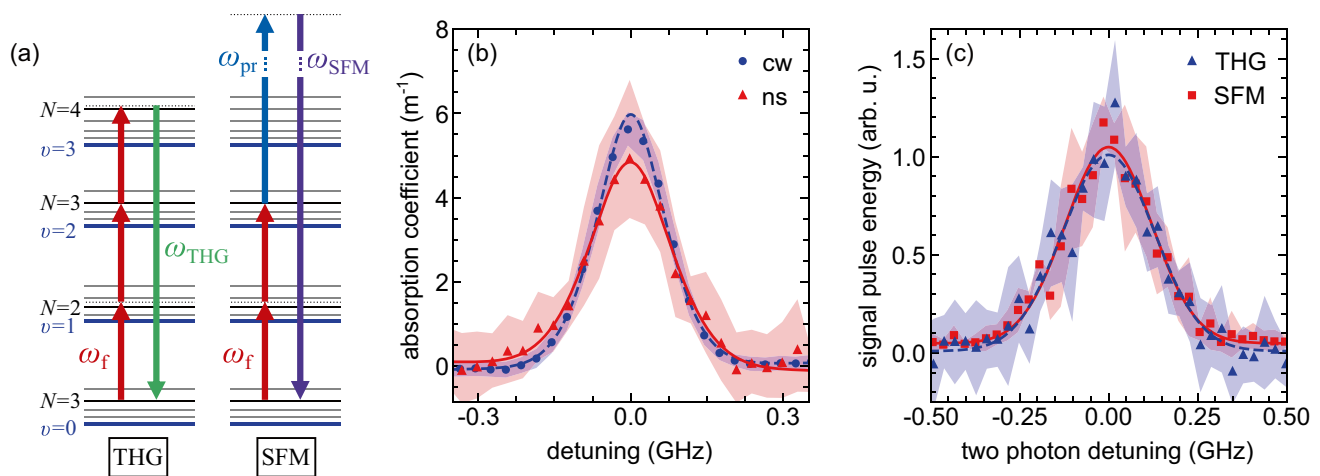
Fig. 5 a Level schemes for two-photon resonant THG and SFM among rovibrational states in the electronic ground state of HCl. v and N indicate vibrational and rotational quantum numbers. **b** Absorption coefficient for attenuated and collimated radiation from the (cw) OPO and the (ns) LNB OPA, versus detuning from the P(3) line of $H^{37}Cl$ at 3546.65 nm. The HCl pressure was 0.09 mbar. Lines indicate Gaussian fits. **c** Normalized THG and SFM signal pulse energy versus two-photon detuning at an HCl pressure of 3.9 mbar. The fundamental wavelength was 3533 nm. The fundamental pulse energy was 0.7 mJ for the THG spectrum and 0.8 mJ for the SFM spectrum. The probe pulse energy was 0.6 mJ at 1064 nm. Lines indicate Voigt fits with a fixed Lorentzian component of 54 MHz (FWHM), which corresponds to the collisional broadening at an HCl pressure of 3.9 mbar. Shaded areas indicate the standard deviation for binning of the data points in 30 MHz increments

THG to yield a signal at thrice the fundamental frequency, i.e., a wavelength of 1.178 μm. We tune the OPO/OPA system now in the vicinity of a rovibrational two-photon resonance between the vibrational ground state $v = 0$ and the excited state $v = 2$. This two-photon resonance enhances the THG conversion efficiency. For the experiment, we focus the mid-infrared fundamental radiation from our OPO/OPA system with a pulse energy of 0.7 mJ, a confocal parameter of $b = 6$ cm into the $L = 18$ cm long gas cell. This yields a Gaussian beam profile with an $1/e^2$-radius of ≈ 180 μm. We separate the THG signal from the fundamental field with a Pellin-Broca prism and detect it on an avalanche photodiode (APD, IAG200S6, Laser Components) equipped with an amplifier (DLPCA-200, Femto).

We conduct the measurement at a low HCl pressure of 3.9 mbar. Thus, Doppler broadening with a width of 175 MHz dominates the spectral linewidth of the two-photon resonance. Collisional broadening adds ≈ 54 MHz to the linewidth [25, 28]. As Doppler broadening leads to a Gaussian spectral profile and collisional broadening to a Lorentzian, we expect a Voigt profile of the two-photon resonance with a linewidth of 206 MHz for their combined contribution. We use an approximation to calculate the FWHM of a Voigt profile based on the Gaussian and Lorentzian components [29].

Figure 5c shows the THG signal yield, when we tune the OPO/OPA system across the two-photon resonance. A Voigt profile obviously describes the experimental data well. The observed linewidth is 298 MHz, i.e., larger than the

resonance linewidth. The difference is due to the bandwidth of the mid-infrared laser pulses, which possess a Gaussian spectrum. The fitted Gaussian component of the Voigt profile has a linewidth of 268 MHz. Deconvolution involving thrice the idler bandwidth of 108 MHz yields a Gaussian linewidth of 192 MHz, i.e., close to the expected value for a Doppler broadened line. Thus, the spectral line from THG confirms the narrow bandwidth of the idler pulses.

In an extension of the setup, we also investigated the two-photon resonance by sum frequency mixing (SFM). Figure 1 depicts the coupling scheme: In the molecular gas, we mix the mid-infrared pulses from our OPO/OPA system with some residual near-infrared radiation of our injection-seeded Nd:YAG laser, which we also apply as pump laser for the OPA stages. Due to selection rules, this requires a four-wave mixing process, e.g., involving two photons from the mid-infrared laser and one photon from the near-infrared laser. The resulting SFM signal is at a wavelength of 664 nm, i.e., in the visible regime and easily detectable with silicon-based photodetectors.

For the SFM experiment, we overlap both beams with the same confocal parameter in the gas cell. Dichroic optics separate the SFM signal from fundamental radiation and parasitic processes. The signal is detected on a photo multiplier (R4220, Hamamatsu Photonics). Figure 5c shows the SFM signal yield, when we tune the OPO/OPA system across the same two-photon resonance, which we already discussed for THG above. As in THG, also the SFM signal is enhanced by the two-photon resonance. The Voigt profile

for SFM has a linewidth of 281 MHz. The Gaussian component as a result of the Voigt fit has a bandwidth of 251 MHz, i.e., lower than for THG. Deconvolution involving twice the idler of 108 MHz and once the probe bandwidth of 55 MHz yields a linewidth of 191 MHz, which is very similar to THG. Hence, the SFM experiment confirms the spectral linewidth obtained from the THG measurements. This is no surprise, as both nonlinear processes probe the same two-photon resonance. Moreover, the spectral line from SFM again confirms the narrow spectral linewidth of the idler pulses, as determined from the absorption measurements.

The measurements of nonlinear spectroscopy by THG and SFM clearly demonstrate, that our OPO/OPA setup is very well applicable for such purposes. It provides sufficient pulse energy to drive nonlinear processes for spectrometry and narrow bandwidth close to the Fourier limit enabling large spectral resolution. We note, that in our previous, systematic investigations of THG spectroscopy we also confirmed the broad tunability of the OPO/OPA system across a large wavelength range [28].

4 Summary and conclusion

We demonstrated an all-solid-state light source for nanosecond (ns) laser pulses, with broad tunability in the mid-infrared spectral regime, narrow spectral bandwidth close to the Fourier limit, and pulse energy in the mJ regime. The mid-infrared output of a tunable, continuous wave (cw) singly resonant optical parametric oscillator (OPO) seeds a two-stage optical parametric amplifier (OPA), pumped by an injection-seeded (ns) Nd:YAG laser. The first OPA stage (pre-amplifier), based on a PPLN crystal, generates mid-infrared pulses with pulse energies in the range of 30 μJ. A subsequent second OPA stage (power amplifier), which consists of two bulk LNB crystals in walk-off compensation configuration, further amplifies the idler pulse energy up to 1.7 mJ while maintaining a homogeneous, close-to-Gaussian beam profile. The conversion efficiency in the power amplifier stage with regard to combined idler and signal pulses reaches 20%, yielding several mJ of combined output power. We demonstrated the broad tunability of the laser system for mid-infrared wavelengths between 3.3 and 3.8 μm, while maintaining idler pulse energies beyond 1 mJ. By exchanging the (cw) OPO seed source, the OPA chain is ready to cover an even larger wavelength range between 3.2 and 4.6 μm. We determined a pulse duration of 5.8 ns for the mid-infrared idler pulses by measuring the second harmonic of the corresponding signal pulses. From absorption measurements in hydrogen chloride (HCl), we deduce a narrow spectral bandwidth of 108 MHz for the (ns) idler pulses. This is very close to the Fourier limit, expected at 76 MHz. Finally, we demonstrated the applicability of the OPO/OPA laser system by nonlinear spectroscopy via third harmonic generation (THG) and sum frequency mixing (SFM) enhanced by rovibrational resonances in HCl. The spectral data confirmed reliable tunability and narrow spectral bandwidth.

We conclude, that the combination of high-gain PPLN pre-amplifier and high-energy bulk LNB power amplifier stages is a versatile and efficient way to generate narrow-band, broadly tunable, intense mid-infrared (ns) pulses from a (cw) OPO seed source. It is a rather straightforward extension for the increasing number of commercially available (cw) OPOs in the mid-infrared, which offer broad continuous tunability, single longitudinal mode operation, good beam quality, and large output power. The OPO/OPA system will be an appropriate tool for applications in nonlinear spectroscopy and trace molecule detection.

Declarations

Conflict of interest The authors declare that they have no conflict of interest.

References

1. D. S. Bethune, A. C. Luntz, A laser infrared source of nanosecond pulses tunable from 1.4 to 22 μm. Appl. Phys. B **40**, 107–113 (1986). https://doi.org/10.1007/BF00694784

2. M. Gerhards, High energy and narrow bandwidth mid IR nanosecond laser system. Opt. Commun. **241**, 493–497 (2004). https://doi.org/10.1016/j.optcom.2004.07.035

3. M. Ebrahim-Zadeh, Mid-Infrared Optical Parametric Oscillators and Applications, in: M. Ebrahim-Zadeh, I.T. Sorokina (eds) Mid-Infrared Coherent Sources and Applications, NATO Science for Peace and Security Series B: Physics and Biophysics. Springer, Dordrecht. (2008). https://doi.org/10.1007/978-1-4020-6463-0_10

4. W. R. Bosenberg, L. E. Myers, R. L. Byer, A. Drobshoff, J. I. Alexander, 93% pump depletion, 3.5-W continuous-wave, singly resonant optical parametric oscillator. Opt. Lett. **21**, 1336–1338 (1996). https://doi.org/10.1364/OL.21.001336

5. A.K.Y. Ngai, S.T. Persijn, G. von Basum, F.J. Harren, Automatically tunable continuous-wave optical parametric oscillator for high-resolution spectroscopy and sensitive trace-gas detection. Appl. Phys. B **85**, 173–180 (2006). https://doi.org/10.1007/s00340-006-2362-3

6. M. Vainio, L. Halonen, Mid-infrared optical parametric oscillators and frequency combs for molecular spectroscopy. Phys. Chem. Chem. Phys. **18**, 4266–4294 (2016). https://doi.org/10.1039/C5CP07052J

7. A. Henderson, R. Stafford, Low threshold, singly-resonant CW OPO pumped by an all-fiber pump source. Opt. Express **14**, 767–772 (2006). https://doi.org/10.1364/OPEX.14.000767

8. D.B. Foote, M.J. Cich, W.C. Hurlbut, U. Eismann, A.T. Heiniger, C. Haimberger, High-resolution, broadly-tunable mid-IR spectroscopy using a continuous wave optical parametric oscillator. Opt. Express **29**, 5295–5303 (2021). https://doi.org/10.1364/oe.418287

9. X. Wang, K. Jia, H. Yao, J. Zhou, G. Lv, G. Zhao, Z. Xie, S. Zhu, High-energy single-longitudinal-mode mid-infrared optical parametric amplifier seeded with sheet optical parametric oscillator. AIP Adv. **11**, 065104 (2021). https://doi.org/10.1063/5.0049754

10. W.R. Bosenberg, D.R. Guyer, Broadly tunable, single-frequency optical parametric frequency-conversion system. J. Opt. Soc. Am. B **10**, 1716–1722 (1993). https://doi.org/10.1364/JOSAB.10.001716

11. G. Baxter, Y. He, B. Orr, A pulsed optical parametric oscillator, based on periodically poled lithium niobate (PPLN), for high-resolution spectroscopy. Appl. Phys. B **67**, 753–756 (1998). https://doi.org/10.1007/s003400050576

12. V. Petrov, Frequency down-conversion of solid-state laser sources to the mid-infrared spectral range using non-oxide nonlinear crystals. Prog. Quantum Electron. **42**, 1–106 (2015). https://doi.org/10.1016/j.pquantelec.2015.04.001

13. P.E. Powers, K.W. Aniolek, T.J. Kulp, B.A. Richman, S.E. Bisson, Periodically poled lithium niobate optical parametric amplifier seeded with the narrow-band filtered output of an optical parametric generator. Opt. Lett. **23**, 1886–1888 (1998). https://doi.org/10.1364/OL.23.001886

14. U. Bäder, T. Mattern, T. Bauer, J. Bartschke, M. Rahm, A. Borsutzky, R. Wallenstein, Pulsed nanosecond optical parametric generator based on periodically poled lithium niobate. Opt. Commun. **217**, 375–380 (2003). https://doi.org/10.1016/S0030-4018(02)02342-8

15. A.M. Morrison, T. Liang, G.E. Douberly, Automation of an "Aculight'' continuous-wave optical parametric oscillator. Rev. Sci. Instrum. **84**, 013102 (2013). https://doi.org/10.1063/1.4776179

16. Y. Furukawa, K. Kitamura, S. Takekawa, K. Niwa, H. Hatano, Stoichiometric Mg:LiNbO$_3$ as an effective material for nonlinear optics. Opt. Lett. **23**, 1892–1894 (1998). https://doi.org/10.1364/OL.23.001892

17. G. Arisholm, R. Paschotta, T. Sudmeyer, Limits to the power scalability of high-gain optical parametric amplifiers. J. Opt. Soc. Am. B **21**(3), 578–590 (2003). https://doi.org/10.1364/JOSAB.21.000578

18. D.J. Armstrong, W.J. Alford, T.D. Raymond, A.V. Smith, M.S. Bowers, Parametric amplification and oscillation with walkoff-compensating crystals. J. Opt. Soc. Am. B **14**(2), 460–474 (1997). https://doi.org/10.1364/JOSAB.14.000460

19. A. V. Smith, SNLO nonlinear optics code available from AS-photonics, Albuquerque, NM. https://as-photonics.com/products/snlo/

20. O. Gayer, Z. Sacks, E. Galun, A. Arie, Temperature and wavelength dependent refractive index equations for MgO-doped congruent and stoichiometric LiNbO$_3$. Appl. Phys. B **91**, 343–348 (2008). https://doi.org/10.1007/s00340-008-2998-2

21. Y.S. Kim, R.T. Smith, Thermal Expansion of Lithium Tantalate and Lithium Niobate Single Crystals. J. Appl. Phys. **40**, 4637 (1969). https://doi.org/10.1063/1.1657244

22. D.H. Jundt, Temperature-dependent Sellmeier equation for the index of refraction, n$_e$, in congruent lithium niobate. Opt. Lett. **22**(20), 1553–1555 (1997). https://doi.org/10.1364/OL.22.001553

23. A.A. Stec, T.R. Hull, K. Lebek, J.A. Purser, D.A. Purser, The effect of temperature and ventilation condition on the toxic product yields from burning polymers. Fire Mater. **32**, 49–60 (2007). https://doi.org/10.1002/fam.955

24. X. Ren, R. Sun, H.-H. Chi, X. Meng, Y. Li, Y.A. Levendis, Hydrogen chloride emissions from combustion of raw and torrefied biomass. Fuel **200**, 37–46 (2017). https://doi.org/10.1016/j.fuel.2017.03.040

25. I. E. Gordon, L. S. Rothman, C. Hill, R. V. Kochanov, Y. Tan, P. F. Bernath, M. Birk, V. Boudon, A. Campargue, K. V. Chance, B. J. Drouin, J.-M. Flaud, R. R. Gamache, J. T. Hodges, D. Jacquemart, V. I. Perevalov, A. Perrin, K. P. Shine, M.-A. H. Smith, J. Tennyson, G. C. Toon, H. Tran, V. G. Tyuterev, A. Barbe, A. G. Császár, V. M. Devi, T. Furtenbacher, J. J. Harrison, J.-M. Hartmann, A. Jolly, T. J. Johnson, T. Karman, I. Kleiner, A. A. Kyuberis, J. Loos, O. M. Lyulin, S. T. Massie, S. N. Mikhailenko, N. Moazzen-Ahmadi, H. S. P. Müller, O. V. Naumenko, A. V. Nikitin, O. L. Polyansky, M. Rey, M. Rotger, S. W. Sharpe, K. Sung, E. Starikova, S. A. Tashkun, J. Vander Auwera, G. Wagner, J. Wilzewski, P. Wcisło, S. Yu, E. J. Zak, The HITRAN2016 molecular spectroscopic database. J. Quant. Spectrosc. Radiat. Transfer **203**, 3–69 (2017). https://doi.org/10.1016/j.jqsrt.2017.06.038

26. A.S. Pine, A. Fried, Self-broadening in the fundamental bands of HF and HCl. J. Mol. Spectrosc. **114**, 148–162 (1985). https://doi.org/10.1016/0022-2852(85)90344-3

27. P.L. Varghese, R.K. Hanson, Collisional narrowing effects on spectral line shapes measured at high resolution. Appl. Opt. **23**, 2376–2385 (1984). https://doi.org/10.1364/ao.23.002376

28. J.F. Kinder, F. Cipura, T. Halfmann, Detection of HCl molecules by resonantly enhanced third-harmonic generation, driven by midinfrared laser pulses. Phys. Rev. A **103**, 052808 (2021). https://doi.org/10.1103/PhysRevA.103.052808

29. J.J. Olivero, R.L. Longbothum, Empirical fits to the Voigt line width: A brief review. J. Quant. Spectrosc. Radiat. Transfer **17**, 233–236 (1977). https://doi.org/10.1016/0022-4073(77)90161-3